MOX-Report No. 22/2017

Biomembrane modeling with Isogeometric Analysis

Bartezzaghi, A.; Dede', L.; Quarteroni, A.

MOX, Dipartimento di Matematica
Politecnico di Milano, Via Bonardi 9 - 20133 Milano (Italy)

mox-dmat@polimi.it http://mox.polimi.it

BIOMEMBRANE MODELING WITH ISOGEOMETRIC ANALYSIS

ANDREA BARTEZZAGHI*, LUCA DEDÈ†, AND ALFIO QUARTERONI†‡

Abstract. We consider the numerical approximation of lipid biomembranes, including red blood cells, described through the Canham–Helfrich model, according to which the shape minimizes the bending energy under area and volume constraints. Energy minimization is performed via L^2-gradient flow of the Canham–Helfrich energy using two Lagrange multipliers to weakly enforce the constraints. This yields a highly nonlinear, high order, time dependent geometric Partial Differential Equation (PDE). We represent the biomembranes as single-patch NURBS closed surfaces. We discretize the geometric PDEs in space with NURBS-based Isogeometric Analysis and in time with Backward Differentiation Formulas. We tackle the nonlinearity in our formulation through a semi-implicit approach by extrapolating, at each time level, the geometric quantities of interest from previous time steps. We report the numerical results of the approximation of the Canham–Helfrich problem on ellipsoids of different aspect ratio, which lead to the classical biconcave shape of lipid vesicles at equilibrium. We show that this framework permits an accurate approximation of the Canham–Helfrich problem, while being computationally efficient.

Key words. Biomembrane, Canham–Helfrich energy, Geometric Partial Differential Equation, NURBS, Isogeometric Analysis, Backward Differentiation Formulas, Lagrange multipliers

AMS subject classifications. 65M60, 53C44, 35Q92

1. Introduction.

A lipid *vesicle*, as e.g. a red blood cell, is a biomembrane consisting of a lipid bilayer, made of molecules with a hydrophilic head group and two hydrophobic hydrocarbon chains, which spontaneously aggregate in closed shapes when set in an aqueous environment [1]. Lipid bilayers are of great interest in biology since they are fundamental components of the boundary of cells and organelles [2]; a wide variety of mathematical models describing their shape and dynamic behavior has been proposed in recent years. In general, they can be classified into microscopic discrete molecular based models, as for example in [3, 4, 5, 6], multiscale models, as in [7, 8, 9], and macroscopic continuum models, e.g. in [10, 11, 12, 13, 14, 15]. A common assumption consists in treating the membranes as surfaces embedded in the 3D space since the combined layer thickness is small compared to the diameter of the vesicle; for example, considering red blood cells, the membrane thickness is less than 100 nm, while their diameter is about 8 µm wide [16]. In these mathematical models the bending elasticity (or curvature energy) is the driving factor for the configuration of the vesicles.

In this paper, we consider the Canham–Helfrich energy, introduced in the seminal works [17, 18] as one of the simplest, but widely recognized models for expressing the biomembrane's bending energy. At equilibrium — i.e. assuming a stable environment with fixed temperature and osmotic pressure — the vesicles tend to assume shapes which minimize such energy. Vesicles also preserve the enclosed volume — since the membrane is impermeable — and the surface area, as the amount of lipid molecules does not change and the resistance of the membrane to stretching or compression is much higher than its rigidity to bending [1]. Therefore, the minimization of the bending energy is coupled with two geometric constraints enforcing fixed area and volume. The mathematical models based on the minimization of the bending

*CMCS – Chair of Modeling and Scientific Computing, EPFL – École Polytechnique Fédérale de Lausanne, Switzerland (andrea.bartezzaghi@epfl.ch, alfio.quarteroni@epfl.ch).

†MOX – Modeling and Scientific Computing, Department of Mathematics, Politecnico di Milano, Italy (luca.dede@polimi.it, alfio.quarteroni@polimi.it)

energy for the vesicle shape modeling are usually approximated numerically with finite element-based discretizations of the membrane surface, as in [10, 11, 12, 13], or by using phase field approaches, as e.g. in [19, 20, 21]. In this work, we propose a numerical approximation of the Canham–Helfrich energy minimization by means of NURBS-based Isogeometric Analysis (IGA) in the framework of the Galerkin method. IGA is a discretization technique for PDEs based on the isoparametric concept, according to which the basis functions used to represent the domain are then used to build the trial function space for the solutions of the PDEs [22, 23]. We represent the biomembrane surface as single-patch NURBS [24], which are capable of describing complex geometries with a relatively low amount of Degrees of Freedom (DOFs). In addition to the advantage of not requiring a separate meshing process and being able to represent the geometry exactly even at the coarsest level of refinement, IGA is suitable also for the spatial approximation of high order PDEs [25], as function spaces can be built of basis functions continuous, together with their derivatives of "high" order, on closed surfaces (see [26]), and especially convenient for the approximation of geometric PDEs [27].

Following our previous work [27], we propose a formulation based on the velocity and the normal velocity of points on the surface, however endowed with two additional Lagrange multipliers to handle the area and volume constraints. We discretize the PDEs in time by employing high order Backward Differentiation Formulas (BDF) [28, 29], with explicit treatment of the extrapolated geometric quantities [30, 27] in order to yield a semi-implicit formulation. To treat the constraints at each time step, we consider two schemes: the first one is an adaptation of the iterative scheme employed in [31, 13] to deal with the nonlinear equations enforcing the constraints. For the second one, we propose the fulfillment of the constraints on the extrapolated surface, relying on the accurate geometric representation given by NURBS-based IGA. Finally, we apply the proposed numerical formulation on surfaces with initial ellipsoidal shapes of different aspect ratios, for which the minimization of the Canham–Helfrich energy under area and volume conservations leads to the typical biconcave shape of red blood cells.

This paper is organized as follows: in Section 2 we introduce a mathematic model based on the Canham–Helfrich energy for describing the shape of vesicles at equilibrium; we discuss the spatial and temporal discretization of the PDEs in Section 3, with the proposed schemes for enforcing the area and volume constraints in Sections 3.3.1 and 3.3.2; then, we report and discuss numerical results for red blood cells in Section 4. Conclusions follow.

2. Mathematical Model. In this paper we adopt the same notation of [27]. Let us consider a vesicle represented by a compact, connected, oriented and smooth closed surface $\Omega \subset \mathbb{R}^3$, defined from a parametric domain $\widehat{\Omega} \in \mathbb{R}^2$ by means of the geometrical mapping $\mathbf{X} : \widehat{\Omega} \to \Omega$, which we assume to be invertible almost everywhere (a.e.) in $\widehat{\Omega}$. We introduce the energy J_W defined as:

$$J_W(\Omega) = \frac{1}{2}\, k_c \int_\Omega (H - H_0)^2 d\Omega, \tag{2.1}$$

which is known as the Willmore energy in the case $k_c = 1$ and $H_0 = 0$ [32]. Then, the bending energy J_B associated with the surface Ω reads [1]:

$$J_B(\Omega) = J_W(\Omega) + \frac{1}{2} k_g \int_\Omega K \, d\Omega. \tag{2.2}$$

In Eqs. (2.1) and (2.2), k_c and k_g are positive constants representing bending rigidities, while H and K denote the total mean curvature and Gauss curvatures, respectively, defined as $H = \kappa_1 + \kappa_2$ and $K = \kappa_1\kappa_2$. The principal curvatures κ_1 and κ_2 on the surface Ω are obtained as the two non-zero eigenvalues of the shape operator $\mathcal{H} = \nabla_\Omega \mathbf{n}_\Omega$ in each point of the surface Ω, with $\mathbf{n}_\Omega$ being the outward pointing unit normal to the surface. The constant H_0 in Eq. (2.1) describes the spontaneous curvature of the vesicle and it is used to model an unbalance of the membrane due to a different chemical environment on the two sides of the vesicle or different chemical composition of the two layers [1, 33, 34, 35]. For simplicity, in this work, we consider the case without spontaneous curvature, i.e. $H_0 = 0$. This choice leads to a problem involving a slightly simplified shape derivative of the energy J_B; this however does not essentially impact on the outcomes of this work. In virtue of the Gauss-Bonnet theorem [36], the second energy term in Eq. (2.2) does not depend on the shape of Ω, but it is a topological invariant which only depends on the genus of the surface. As in this work we do not consider topological changes, the second term in Eq. (2.2) will be neglected (by setting $k_g = 0$).

To simplify the notation, we introduce the identity function $\mathbf{x} : \Omega \to \mathbb{R}^3$ on Ω, defined as $\mathbf{x}(\mathbf{X}(\boldsymbol{\xi})) = \mathbf{X}(\boldsymbol{\xi})$, for $\boldsymbol{\xi} \in \widehat{\Omega}$. Then, we express the area J_A of the closed surface Ω as:

$$J_A(\Omega) = \int_\Omega 1 \, d\Omega \tag{2.3}$$

and the volume J_V of the region of the physical space enclosed by Ω as:

$$J_V(\Omega) = \int_\Omega \mathbf{x} \cdot \mathbf{n}_\Omega \, d\Omega. \tag{2.4}$$

To enforce the area and volume constraints, we augment the energy in Eq. (2.2) by means of Lagrange multipliers, obtaining the Canham–Helfrich energy J_{CH} [12]:

$$J_{CH}(\Omega, \delta p, \Pi_\Omega) = J_W(\Omega) + \Pi_\Omega \Big(J_A(\Omega) - J_A(\Omega_0) \Big) + \delta p \Big(J_V(\Omega) - J_V(\Omega_0) \Big), \tag{2.5}$$

where Ω_0 is a reference (or initial) surface and Π_Ω and δp are the Lagrange multipliers associated with the area and volume constraints, respectively. More precisely, δp is interpreted as an osmotic pressure jump across the inner and outer sides of the biomembrane, while Π_Ω as the tensile stress required to maintain the inextensibility of the membrane [34, 37].

2.1. Energy minimization. We study the equilibrium shapes of the biomembranes by minimizing the Canham–Helfrich energy J_{CH} of Eq. (2.5); with this aim, we formulate the *Canham–Helfrich flow problem* as the L^2-gradient flow of J_{CH}. Given an initial surface $\Omega_0 \subset \mathbb{R}^3$, find, for all $t \in (0, T)$, $\mathbf{x} \in V_t$, $\Pi_{\Omega t} \in \mathbb{R}$, and $\delta p_t \in \mathbb{R}$ such that

$$\begin{cases} (\dot{\mathbf{x}}, \boldsymbol{\varphi})_{L^2(\Omega_t)} = -dJ_{CH}\left(\Omega(\mathbf{x}), \Pi_{\Omega t}, \delta p_t; \boldsymbol{\varphi}\right) & \forall \boldsymbol{\varphi} \in V_t, \\ J_A(\Omega_t) = J_A(\Omega_0), \qquad J_V(\Omega_t) = J_V(\Omega_0), & \\ \mathbf{x}(0) = \mathbf{x}_0 & \text{in } \Omega_0, \end{cases} \tag{2.6}$$

where $V_t := [H^2(\Omega_t)]^3$, $\dot{\mathbf{x}}$ refers to the material derivative of $\mathbf{x}$, and dJ_{CH} is the Gâteaux derivative of J_{CH}. The material derivative of a general function $\boldsymbol{\varphi}$ in a

moving system of reference is defined as $\dot{\boldsymbol{\varphi}} = \frac{\partial \boldsymbol{\varphi}}{\partial t} + \mathbf{v} \cdot \nabla_\Omega \boldsymbol{\varphi}$, where $\mathbf{v}$ is the velocity of the system of reference. We have that $\dot{\mathbf{x}} = \frac{\partial \mathbf{x}}{\partial t} + \mathbf{v} \cdot \nabla_\Omega \mathbf{x}$; therefore, $\dot{\mathbf{x}} = \mathbf{v}$ since $\frac{\partial \mathbf{x}}{\partial t} = \mathbf{0}$ and $\nabla_\Omega \mathbf{x} = \mathbb{I}$, where $\mathbb{I}$ is the second order identity tensor [38]. The Gâteaux derivative (or shape derivative) of J_{CH} with respect to the direction $\boldsymbol{\varphi} \in V_t$ reads [37]:

$$dJ_{CH}(\Omega, \Pi_\Omega, \delta p; \boldsymbol{\varphi}) = dJ_W(\Omega; \boldsymbol{\varphi}) + \Pi_\Omega \, dJ_A(\Omega; \boldsymbol{\varphi}) + \delta p \, dJ_V(\Omega; \boldsymbol{\varphi}), \tag{2.7}$$

where the shape derivatives of J_V and J_A along $\boldsymbol{\varphi}$ are given by:

$$dJ_A(\Omega; \boldsymbol{\varphi}) = \int_\Omega H \boldsymbol{\varphi} \cdot \mathbf{n}_\Omega \, d\Omega \tag{2.8}$$

and

$$dJ_V(\Omega; \boldsymbol{\varphi}) = \int_\Omega \boldsymbol{\varphi} \cdot \mathbf{n}_\Omega \, d\Omega, \tag{2.9}$$

respectively. By considering $H_0 = 0$, the shape derivative of the energy J_W reads [39, 38]:

$$dJ_W(\Omega; \boldsymbol{\varphi}) = k_c \int_\Omega \left[-H \left(\frac{1}{2} H^2 - 2K \right) - \Delta_\Omega H \right] \boldsymbol{\varphi} \cdot \mathbf{n}_\Omega \, d\Omega, \tag{2.10}$$

where Δ_Ω is the Laplace–Beltrami operator on the surface Ω [26]. By using Eqs. (2.8), (2.9), and (2.10) in Eq. (2.7) we finally obtain:

$$dJ_{CH}(\Omega, \Pi_\Omega, \delta p; \boldsymbol{\varphi}) = \int_\Omega \left\{ k_c \left[-H \left(\frac{1}{2} H^2 - 2K \right) - \Delta_\Omega H \right] + \Pi_\Omega H + \delta p \right\} \boldsymbol{\varphi} \cdot \mathbf{n}_\Omega \, d\Omega. \tag{2.11}$$

In particular, the Canham–Helfrich flow problem in strong form reads: find, for all $t \in (0, T)$, $\Omega_t \subset \mathbb{R}^3$, $\Pi_{\Omega t} \in \mathbb{R}$, and $\delta p_t \in \mathbb{R}$ such that

$$\begin{cases} \dot{\mathbf{x}} = - \left\{ k_c \left[-H \left(\frac{1}{2} H^2 - 2K \right) - \Delta_{\Omega_t} H \right] + \Pi_{\Omega t} H + \delta p_t \right\} \mathbf{n}_{\Omega_t} & \text{in } \Omega_t, \\ J_A(\Omega_t) = J_A(\Omega_0), \qquad J_V(\Omega_t) = J_V(\Omega_0), & \\ \mathbf{x}(0) = \mathbf{x}_0 & \text{in } \Omega_0. \end{cases} \tag{2.12}$$

In [27] we proposed a formulation with the velocity $\mathbf{v} = \dot{\mathbf{x}}$ and the normal velocity v as unknowns of the Willmore flow problem. Since the Canham–Helfrich flow represents an extension of the Willmore flow problem with area and volume constraints, we apply the same idea in this work. In particular, we consider the following weak

formulation:

find, for all $t \in (0,T)$, $\mathbf{x} \in V_t$, $v \in W_t$, $\Pi_{\Omega t} \in \mathbb{R}$, and $\delta p_t \in \mathbb{R}$ such that

$$
\begin{cases}
\displaystyle\int_{\Omega_t} \dot{\mathbf{x}} \cdot \boldsymbol{\varphi}\, d\Omega_t - \int_{\Omega_t} v\, \mathbf{n}_{\Omega_t} \cdot \boldsymbol{\varphi}\, d\Omega_t = 0 & \forall \boldsymbol{\varphi} \in V_t, \\
\displaystyle\int_{\Omega_t} v\psi\, d\Omega_t + k_c \int_{\Omega_t} (\Delta_{\Omega_t}\mathbf{x} \cdot \mathbf{n}_{\Omega_t})\Delta_{\Omega_t}\psi\, d\Omega_t & \\
\qquad \displaystyle + k_c \int_{\Omega_t} (\Delta_{\Omega_t}\mathbf{x} \cdot \mathbf{n}_{\Omega_t}) \left(\frac{1}{2}H^2 - 2K\right)\psi\, d\Omega_t & \\
\qquad \displaystyle + \Pi_{\Omega t} \int_{\Omega_t} H\, \psi\, d\Omega_t + \delta p_t \int_{\Omega_t} \psi\, d\Omega_t = 0 & \forall \psi \in W_t, \\
\displaystyle\int_{\Omega_t} H\, \mathbf{x} \cdot \mathbf{n}_{\Omega_t}\, d\Omega_t = A_0, \qquad \int_{\Omega_t} \mathbf{x} \cdot \mathbf{n}_{\Omega_t}\, d\Omega_t = V_0, & \\
\mathbf{x}(0) = \mathbf{x}_0, \qquad v(0) = v_0, &
\end{cases}
\tag{2.13}
$$

where we used the relation $H\mathbf{n}_{\Omega_t} = -\Delta_{\Omega_t}\mathbf{x}$ in Ω_t and initial area $A_0 = J_A(\Omega_0)$ and volume $V_0 = J_V(\Omega_0)$. In particular, we consider, for any given $t \in (0,T)$, the function spaces $V_t = \left[H^2(\Omega_t)\right]^3$ and $W_t = H^2(\Omega_t)$, since the formulation of Eq. (2.13) involves second order surface differential operators applied to the trial and test functions.

3. Numerical Approximation. We consider the numerical approximation of problem (2.13). In this section, we introduce both the spatial and time discretizations and we compare two numerical approaches to enforce the area and volume constraints through Lagrange multipliers.

3.1. Spatial discretization. We spatially discretize problem (2.13) by means of a Galerkin method using NURBS-based IGA subspaces [22, 23]. Specifically, we consider the family of surfaces $\{\Omega_t\}_{t\in(0,T)}$ to be represented by single patch NURBS, as in [26, 27, 40]. The main details about the construction of NURBS basis and their properties are provided in [22, 24].

With NURBS, the geometric mapping $\mathbf{X} : \widehat{\Omega} \to \mathbb{R}^3$ introduced in Sect. 2 takes the form:

$$
\mathbf{X}(\boldsymbol{\xi}) = \sum_{i=1}^{n_{bf}} \widehat{R}_i(\boldsymbol{\xi})\mathbf{P}_i,
\tag{3.1}
$$

where $\widehat{R}_i(\boldsymbol{\xi})$ are the NURBS basis functions, n_{bf} is their number, and $\mathbf{P}_i \in \mathbb{R}^3$ are the control points in the physical space $\mathbb{R}^3$. We define the NURBS function space $\widehat{\mathcal{N}}_h$ over the parametric domain $\widehat{\Omega}$ and the function space $\mathcal{N}_h$ over the physical domain Ω as:

$$
\widehat{\mathcal{N}}_h := \operatorname{span}\left\{\widehat{R}_i, \quad i = 1, \ldots, n_{bf}\right\}
\tag{3.2}
$$

and

$$
\mathcal{N}_h := \operatorname{span}\left\{\widehat{R}_i(\boldsymbol{\xi}) \circ \mathbf{X}^{-1}(\boldsymbol{\xi}), \quad i = 1, \ldots, n_{bf}\right\},
\tag{3.3}
$$

respectively. At this point, we consider the discretization of problem (2.13). The function spaces $\mathcal{N}_h$ and $\widehat{\mathcal{N}}_h$ are also used to build the trial and the test function spaces.

In particular, for any $t \in (0,T)$, we choose $V_{t,h} := V_t \cap \mathcal{N}_h$ and $W_{t,h} := W_t \cap \mathcal{N}_h$ as trial and test function spaces. Therefore, for all $t \in (0,T)$, we look for solutions:

$$\mathbf{x}_h(t) = \sum_{i=1}^{n_{bf}} \left(\widehat{R}_i \circ \mathbf{X}^{-1} \right) \mathbf{P}_i(t), \tag{3.4}$$

where the control points $\mathbf{P}_i : (0,T) \to \mathbb{R}^3$, for $i = 1, \dots, n_{bf}$, defining the surface Ω_t through the geometric mapping (3.1), represent the unknowns of our problem. Hence, the semi-discrete problem reads:

(3.5)

find, for all $t \in (0,T)$, $\mathbf{x}_h \in V_{t,h}$, $v \in W_{t,h}$, $\Pi_{\Omega t} \in \mathbb{R}$, and $\delta p_t \in \mathbb{R}$ such that

$$\begin{cases} \displaystyle\int_{\Omega_t} \dot{\mathbf{x}}_h \cdot \boldsymbol{\varphi}_h \, d\Omega_t - \int_{\Omega_t} v_h \mathbf{n}_{\Omega_t} \cdot \boldsymbol{\varphi}_h \, d\Omega_t = 0 & \forall \boldsymbol{\varphi}_h \in V_{t,h}, \\ \displaystyle\int_{\Omega_t} v_h \psi_h \, d\Omega_t + k_c \int_{\Omega_t} (\Delta_{\Omega_t} \mathbf{x}_h \cdot \mathbf{n}_{\Omega_t}) \Delta_{\Omega_t} \psi_h \, d\Omega_t \\ \qquad\qquad + k_c \displaystyle\int_{\Omega_t} (\Delta_{\Omega_t} \mathbf{x}_h \cdot \mathbf{n}_{\Omega_t}) \left(\frac{1}{2} H_h^2 - 2K_h \right) \psi_h \, d\Omega_t \\ \qquad\qquad + \Pi_{\Omega t} \displaystyle\int_{\Omega_t} H_h \, \psi_h \, d\Omega_t + \delta p_t \int_{\Omega_t} \psi_h \, d\Omega_t = 0 & \forall \psi_h \in W_{t,h}, \\ \displaystyle\int_{\Omega_t} H_h \, \mathbf{x}_h \cdot \mathbf{n}_{\Omega_t} \, d\Omega_t = A_0, \qquad \int_{\Omega_t} \mathbf{x}_h \cdot \mathbf{n}_{\Omega_t} \, d\Omega_t = V_0, \\ \mathbf{x}_h(0) = \mathbf{x}_0, \qquad v_h(0) = v_0, \end{cases}$$

where H_h and K_h are the mean and the Gauss curvatures of the surface defined by the approximated solution $\mathbf{x}_h$. We remark that, since problem (3.5) involves second order surface differential operators, we require the function spaces $V_{t,h}$ and $W_{t,h}$ to host basis functions which are at least C^1-continuous a.e. on Ω_t. We deal with single-patch NURBS closed surfaces, for which usually the basis functions describing the geometry are globally just C^0-continuous over the surface [22]. Therefore, we need to transform the NURBS basis functions which build both the geometry and the approximation function space into periodic NURBS basis, with the required global continuity on the surface Ω_t. Nevertheless, a subparametric approach as described in [26] cannot be used since the control points $\{\mathbf{P}_i\}_{i=0}^{n_{bf}}$ describing the geometry are also the control variables of the problem, hence the same function space has to be used for both the geometry and the approximated solution. Therefore, we still use periodic NURBS function spaces, but with coherent transformations of the control points. Details about this method and the construction of periodic NURBS function spaces are reported in [27].

3.2. Time discretization. Regarding problem (3.5), we highlight that all the geometric quantities involved in the formulation (the curvatures H_h and K_h, the normal $\mathbf{n}_{\Omega_t}$, and the domain Ω_t itself) depend on the unknown $\mathbf{x}_h$, as well as the function spaces $V_{t,h}$ and $W_{t,h}$ and the differential operators. Hence, we have that problem (3.5) is nonlinear. In literature [12, 13, 10, 38, 41] problems involving geometric PDEs are usually discretized in time with semi-implicit, first order schemes: at each time instance the geometrical terms are evaluated using the solution computed at the previous time instance, thus leading to the solution of a linear system at each

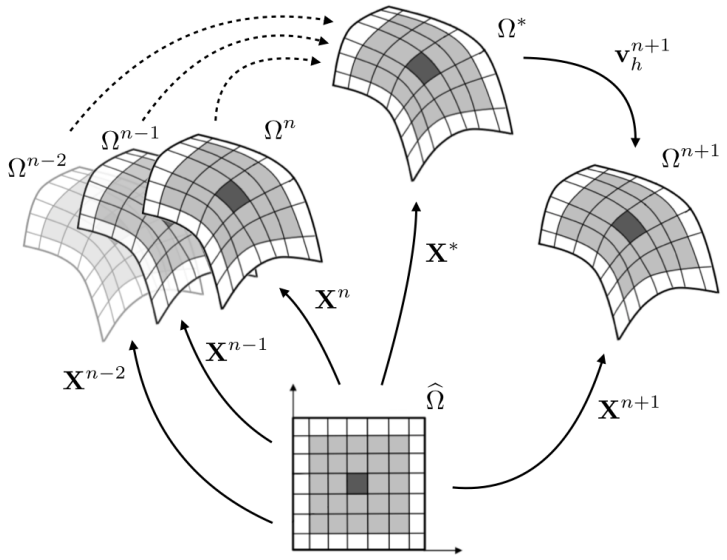

Figure 1: Scheme of the geometric mappings involved in the discretization of Eq. (3.13). In this example, we assume that a BDF scheme of order $k = 3$ is used for the time discretization. We define the approximated surfaces of the current and previous 2 time instances Ω_n, Ω_{n-1}, and Ω_{n-2} from the parametric domain $\widehat{\Omega}$ through the geometric mappings $\mathbf{X}_h^n$, $\mathbf{X}_h^{n-1}$, and $\mathbf{X}_h^{n-2}$, respectively. With a linear combination of these, we define the mapping $\mathbf{X}^*$ for the extrapolated surface Ω_*. Then, we solve the problem on the extrapolated surface, thus obtaining the velocity $\mathbf{v}_h^{n+1}$. The surface Ω_{n+1} at time instance $n+1$, defined through the mapping $\mathbf{X}_h^{n+1}$, is computed from the extrapolated surface Ω_* by means of the approximated velocity $\mathbf{v}_h^{n+1}$.

time step. Instead, in this work, for the temporal discretization of the PDEs we use the high order implicit Backward Differentiation Formulas (BDF) [28], following [27].

We consider the time interval $[0, T]$ and we divide it into $N > 0$, for $N \in \mathbb{N}$, time steps with fixed size Δt such that $t_n = n\Delta t$, with $n = 0, \dots, N$. The approximate surface Ω_{n+1} at time instance t_n is the NURBS surface defined by the mapping:

$$\mathbf{X}_h^{n+1}(\boldsymbol{\xi}) = \sum_{i=1}^{n_{bf}} \widehat{R}_i(\boldsymbol{\xi}) \mathbf{P}_i^{n+1}, \tag{3.6}$$

where $\mathbf{P}_i^{n+1}$, for $i = 1, \dots, n_{bf}$, are the control point coordinates computed at the time instance t_{n+1}. A k-th order BDF approximation of the time derivative $\dot{\mathbf{X}}_h^{n+1}$ reads:

$$\dot{\mathbf{X}}_h^{n+1} \approx \frac{1}{\Delta t} \left(\alpha_0 \mathbf{X}_h^{n+1} - \sum_{i=1}^{k} \alpha_i \mathbf{X}_h^{n+1-i} \right), \tag{3.7}$$

for $n \geq k - 1$, with the coefficients $\alpha_i \in \mathbb{R}$, for $i = 0, \dots, k$, suitably chosen for an approximation of the k-th order. In order to avoid to solve a nonlinear system of equations, we treat the geometric terms in a semi-implicit manner, i.e. we use an extrapolation (of the same order k as the BDF scheme) from the previous time

steps [30, 42]. Firstly, we build the extrapolated surface Ω_*, defined by the NURBS mapping:

$$\mathbf{X}_h^*(\boldsymbol{\xi}) = \sum_{i=1}^{n_{bf}} \widehat{R}_i(\boldsymbol{\xi})\mathbf{P}_i^*, \tag{3.8}$$

where P_i^*, for $i = 1, \dots, n_{bf}$, are the control points extrapolated from the previous k time instances, reading [28]:

$$P_i^* = \sum_{j=1}^{k} \beta_j \mathbf{P}_i^{n+1-j}, \tag{3.9}$$

for $i = 1, \dots n_{bf}$, with $\beta_j \in \mathbb{R}$, for $j = 1, \dots, k$, being appropriate coefficients guaranteeing an extrapolation of the k-th order. Then, we rewrite the problem to be solved such that it lies on the extrapolated surface, i.e. the unknowns become functions defined on Ω_*, as well as the integrals and the geometric quantities. Therefore, following Eq. (3.7), we approximate the time derivative of the identity function $\mathbf{x}_h^{n+1}$, defined on Ω_*, as:

$$\dot{\mathbf{x}}_h^{n+1} \approx \frac{1}{\Delta t}\left[\alpha_0 \mathbf{x}_h^{n+1} - \sum_{i=1}^{k} \alpha_i (\mathbf{x}_h^{n+1-i} \circ \mathbf{X}_h^{n+1-i}) \circ (\mathbf{X}_h^*)^{-1}\right], \tag{3.10}$$

for $n \geq k-1$. Then, we introduce the velocity $\mathbf{v}_h^{n+1} : \Omega_* \to \mathbb{R}^3$ at time instance t_{n+1}, defined as:

$$\mathbf{v}_h^{n+1} := \alpha_0 \frac{\mathbf{x}_h^{n+1} - \mathbf{x}_h^{bdf,n}}{\Delta t}, \tag{3.11}$$

where $\mathbf{x}_h^{bdf,n} : \Omega_* \to \mathbb{R}^3$ is defined as:

$$\mathbf{x}_h^{bdf,n} := \sum_{i=1}^{k} \frac{\alpha_i}{\alpha_0} (\mathbf{x}_h^{n+1-i} \circ \mathbf{X}_h^{n+1-i}) \circ (\mathbf{X}_h^*)^{-1}, \tag{3.12}$$

for $n \geq k-1$. Finally, the time discretization of problem (3.5) yields the fully discrete

problem:

(3.13)

find, for $n = 0, \dots, N-1$, $\mathbf{v}_h^{n+1} \in V_h^*$, $v_h^{n+1} \in W_h^*$, $\Pi_\Omega^{n+1} \in \mathbb{R}$, and $\delta p^{n+1} \in \mathbb{R}$ s.t.

$$
\begin{cases}
\displaystyle\int_{\Omega_*} \mathbf{v}_h^{n+1} \cdot \boldsymbol{\varphi}_h \, d\Omega_* - \int_{\Omega_*} v_h^{n+1} \, \mathbf{n}_{\Omega_*} \cdot \boldsymbol{\varphi}_h \, d\Omega_* = 0 & \forall \boldsymbol{\varphi}_h \in V_h^*, \\
\displaystyle\int_{\Omega_*} v_h^{n+1} \, \psi_h \, d\Omega_* + k_c \frac{\Delta t}{\alpha_0} \int_{\Omega_*} (\Delta_{\Omega_*} \mathbf{v}_h^{n+1} \cdot \mathbf{n}_{\Omega_*}) \Delta_{\Omega_*} \psi_h \, d\Omega_* \\
\qquad + k_c \frac{\Delta t}{\alpha_0} \displaystyle\int_{\Omega_*} \left[\frac{1}{2} (H_h^*)^2 - 2K_h^* \right] (\Delta_{\Omega_*} \mathbf{v}_h^{n+1} \cdot \mathbf{n}_{\Omega_*}) \psi_h \, d\Omega_* \\
\qquad + \Pi_\Omega^{n+1} \displaystyle\int_{\Omega_*} H_h^* \, \psi_h \, d\Omega_* + \delta p^{n+1} \int_{\Omega_*} \psi_h \, d\Omega_* \\
\qquad = -k_c \displaystyle\int_{\Omega_*} \left(\Delta_{\Omega_*} \mathbf{x}_h^{bdf,n} \cdot \mathbf{n}_{\Omega_*} \right) \Delta_{\Omega_*} \psi_h \, d\Omega_* \\
\qquad - k_c \displaystyle\int_{\Omega_*} \left[\frac{1}{2} (H_h^*)^2 - 2K_h^* \right] \left(\Delta_{\Omega_*} \mathbf{x}_h^{bdf,n} \cdot \mathbf{n}_{\Omega_*} \right) \psi_h \, d\Omega_*, & \forall \psi_h \in W_h^*, \\
\displaystyle\int_{\Omega_{n+1}} H_h^{n+1} \, \mathbf{x}_h^{n+1} \cdot \mathbf{n}_{\Omega_{n+1}} \, d\Omega_{n+1} = A_0, \qquad \int_{\Omega_{n+1}} \mathbf{x}_h^{n+1} \cdot \mathbf{n}_{\Omega_{n+1}} \, d\Omega_{n+1} = V_0, \\
\mathbf{v}_h^0 = \mathbf{v}_{0,h}, \qquad v_h^0 = v_{0,h}, \qquad \mathbf{x}_h^{bdf,0} = \mathbf{x}_{0,h}^{bdf,n},
\end{cases}
$$

where V_h^* and W_h^* correspond to the function spaces $V_{t,h}$ and $W_{t,h}$ built on Ω_*, respectively. Problem (3.13) is still nonlinear since we are enforcing the constraints on the surface Ω_{n+1}. In Sect. 3.3 we will discuss how to recover a linear (semi-implicit) formulation of the problem by appropriate handling of the constraints. After having computed the velocity $\mathbf{v}_h^{n+1}$, we obtain the new mapping $\mathbf{x}_h^{n+1} : \Omega_* \to \mathbb{R}^3$ as:

$$
\mathbf{x}_h^{n+1} = \mathbf{x}_h^{bdf,n} + \frac{\Delta t}{\alpha_0} \mathbf{v}_h^{n+1}, \tag{3.14}
$$

corresponding to the new geometrical mapping $\mathbf{X}_h^{n+1}$, which defines the new surface Ω_{n+1}. In Figure 1 we report a sketch of the scheme leading to the computation of the surface Ω_{n+1}, to highlight the time advancing procedure described in this section. We refer the interested reader to [27] for a discussion about the benefits of using this high order time discretization scheme with extrapolation in combination with the high order spatial discretization given by IGA.

3.3. Enforcement of the area and volume constraints. To enforce the area and volume constraints of problem (3.13) we propose two approaches. The first one is an adaptation of the iterative scheme proposed in [12, 13] to our context based on IGA and BDF discretizations, which is able to enforce the area and volume constraints to machine precision. Then, we propose a second approach based on the approximation of the constraints; while being not exact, it is however more convenient from a computational point of view.

3.3.1. Constraints enforcement: scheme C-1. We assume for the time being that the Lagrange multipliers $\widetilde{\Pi}_\Omega^{n+1}$ and $\delta\widetilde{p}^{n+1}$ are given. Then, we reformulate

problem (3.13) as follows:

(3.15)

find, for $n = 0, \dots, N-1$, $\mathbf{v}_h^{n+1} \in V_h^*$ and $v_h^{n+1} \in W_h^*$ such that

$$
\begin{cases}
\displaystyle\int_{\Omega_*} \mathbf{v}_h^{n+1} \cdot \boldsymbol{\varphi}_h \, d\Omega_* - \int_{\Omega_*} v_h^{n+1} \, \mathbf{n}_{\Omega_*} \cdot \boldsymbol{\varphi}_h \, d\Omega_* = 0 & \forall \boldsymbol{\varphi}_h \in V_h^*, \\
\displaystyle\int_{\Omega_*} v_h^{n+1} \, \psi_h \, d\Omega_* + k_c \frac{\Delta t}{\alpha_0} \int_{\Omega_*} (\Delta_{\Omega_*} \mathbf{v}_h^{n+1} \cdot \mathbf{n}_{\Omega_*}) \Delta_{\Omega_*} \psi_h \, d\Omega_* \\
\qquad + k_c \frac{\Delta t}{\alpha_0} \displaystyle\int_{\Omega_*} \left[\frac{1}{2} (H_h^*)^2 - 2K_h^* \right] (\Delta_{\Omega_*} \mathbf{v}_h^{n+1} \cdot \mathbf{n}_{\Omega_*}) \psi_h \, d\Omega_* \\
\qquad = -k_c \displaystyle\int_{\Omega_*} \left(\Delta_{\Omega_*} \mathbf{x}_h^{bdf,n} \cdot \mathbf{n}_{\Omega_*} \right) \Delta_{\Omega_*} \psi_h \, d\Omega_* \\
\qquad\quad - k_c \displaystyle\int_{\Omega_*} \left[\frac{1}{2} (H_h^*)^2 - 2K_h^* \right] \left(\Delta_{\Omega_*} \mathbf{x}_h^{bdf,n} \cdot \mathbf{n}_{\Omega_*} \right) \psi_h \, d\Omega_* \\
\qquad\quad - \widetilde{\Pi}_\Omega^{n+1} \displaystyle\int_{\Omega_*} H_h^* \, \psi_h \, d\Omega_* - \delta\widetilde{p}^{n+1} \int_{\Omega_*} \psi_h \, d\Omega_*, & \forall \psi_h \in W_h^*,
\end{cases}
$$

with appropriate initial conditions $\mathbf{v}_h^0 = \mathbf{v}_{0,h}$, $v_h^0 = v_{0,h}$, and $\mathbf{x}_h^{bdf,0} = \mathbf{x}_{0,h}^{bdf,n}$. In compact form, system (3.15) reads, for $n = 0, \dots, N-1$, as:

(3.16)

$$
\mathcal{L}(\mathbf{v}_h^{n+1}, v_h^{n+1}; \boldsymbol{\varphi}_h, \psi_h) = \mathcal{F}_W(\boldsymbol{\varphi}_h, \psi_h) + \widetilde{\Pi}_\Omega^{n+1} \mathcal{F}_A(\boldsymbol{\varphi}_h, \psi_h) + \delta\widetilde{p}^{n+1} \mathcal{F}_V(\boldsymbol{\varphi}_h, \psi_h), \qquad \forall \boldsymbol{\varphi}_h \in V_h^*, \forall \psi_h \in W_h^*,
$$

with obvious choice of notation. Because of the linearity of $\mathcal{L}$ with respect to $\mathbf{v}_h^{n+1}$ and v_h^{n+1}, by the superposition of effects we write:

$$
\mathbf{v}_h^{n+1} = \mathbf{v}_{h,W}^{n+1} + \widetilde{\Pi}_\Omega^{n+1} \mathbf{v}_{h,A}^{n+1} + \delta\widetilde{p}^{n+1} \mathbf{v}_{h,V}^{n+1} \tag{3.17}
$$

and

$$
v_h^{n+1} = v_{h,W}^{n+1} + \widetilde{\Pi}_\Omega^{n+1} v_{h,A}^{n+1} + \delta\widetilde{p}^{n+1} v_{h,V}^{n+1}, \tag{3.18}
$$

where $\mathbf{v}_{h,W}^{n+1}$, $v_{h,W}^{n+1}$, $\mathbf{v}_{h,A}^{n+1}$, $v_{h,A}^{n+1}$, $\mathbf{v}_{h,V}^{n+1}$, and $v_{h,V}^{n+1}$ satisfy the following (independent) problems:

$$
\begin{aligned}
&\mathcal{L}(\mathbf{v}_{h,W}^{n+1}, v_{h,W}^{n+1}; \boldsymbol{\varphi}_h, \psi_h) = \mathcal{F}_W(\boldsymbol{\varphi}_h, \psi_h), \\
&\mathcal{L}(\mathbf{v}_{h,A}^{n+1}, v_{h,A}^{n+1}; \boldsymbol{\varphi}_h, \psi_h) = \mathcal{F}_A(\boldsymbol{\varphi}_h, \psi_h), \qquad \forall \boldsymbol{\varphi}_h \in V_h^*, \forall \psi_h \in W_h^* \\
&\mathcal{L}(\mathbf{v}_{h,V}^{n+1}, v_{h,V}^{n+1}; \boldsymbol{\varphi}_h, \psi_h) = \mathcal{F}_V(\boldsymbol{\varphi}_h, \psi_h).
\end{aligned} \tag{3.19}
$$

At this stage, after solving Eqs. (3.19) and using Eq. (3.17), one needs to recover the values of the (unknown) Lagrange multipliers Π_Ω^{n+1} and δp^{n+1}. With this aim, we enforce the area and volume constraints by looking for the zeros of the vector-valued function $\mathbf{f}_c^n : \mathbb{R}^2 \to \mathbb{R}^2$ defined as:

$$
\mathbf{f}_c^n(\widetilde{\Pi}_\Omega, \delta\widetilde{p}) := \begin{bmatrix} J_A(\widetilde{\Omega}_{n+1}(\widetilde{\Pi}_\Omega, \delta\widetilde{p})) - J_A(\Omega_n) \\ J_V(\widetilde{\Omega}_{n+1}(\widetilde{\Pi}_\Omega, \delta\widetilde{p})) - J_V(\Omega_n) \end{bmatrix} = \mathbf{0}, \tag{3.20}
$$

where $\widetilde{\Omega}_{n+1}(\widetilde{\Pi}_\Omega, \delta\widetilde{p})$ is the surface defined by the mapping:

$$\widetilde{\mathbf{x}}_h^{n+1}(\widetilde{\Pi}_\Omega, \delta\widetilde{p}) = \mathbf{x}_h^{bdf,n} + \frac{\Delta t}{\alpha_0}\left(\mathbf{v}_{h,W}^{n+1} + \widetilde{\Pi}_\Omega\, \mathbf{v}_{h,A}^{n+1} + \delta\widetilde{p}\, \mathbf{v}_{h,V}^{n+1}\right), \tag{3.21}$$

dependent on the general Lagrange multipliers $\widetilde{\Pi}_\Omega$ and $\delta\widetilde{p}$. Then, the zeros of $\mathbf{f}_c$ are approximated by using a quasi-Newton method; see [12] for details about the method applied to a parametric FEM-based discretization. In our context, by indicating with $k \in \mathbb{N}$ the iterate index, we have the following algorithm, for all $n = 0, \ldots, N-1$:

1. Set $k = 0$ and initialize $\widetilde{\Pi}_\Omega^{n+1,0}$ and $\delta\widetilde{p}^{n+1,0}$ as the solutions of the following problem:

$$\begin{bmatrix} \displaystyle\int_{\Omega_*} \nabla_{\Omega_*} \cdot \mathbf{v}_{h,A}^{n+1}\, d\Omega_* & \displaystyle\int_{\Omega_*} \nabla_{\Omega_*} \cdot \mathbf{v}_{h,V}^{n+1}\, d\Omega_* \\ \displaystyle\int_{\Omega_*} \mathbf{n}_{\Omega_*} \cdot \mathbf{v}_{h,A}^{n+1}\, d\Omega_* & \displaystyle\int_{\Omega_*} \mathbf{n}_{\Omega_*} \cdot \mathbf{v}_{h,V}^{n+1}\, d\Omega_* \end{bmatrix} \begin{bmatrix} \widetilde{\Pi}_\Omega^{n+1,0} \\ \delta\widetilde{p}^{n+1,0} \end{bmatrix} = \tag{3.22}$$
$$= \begin{bmatrix} -\displaystyle\int_{\Omega_*} \nabla_{\Omega_*} \cdot \mathbf{v}_{h,W}^{n+1}\, d\Omega_* \\ -\displaystyle\int_{\Omega_*} \mathbf{n}_{\Omega_*} \cdot \mathbf{v}_{h,W}^{n+1}\, d\Omega_* \end{bmatrix}.$$

2. Build the surface $\widetilde{\Omega}_{n+1}^k$, defined by the mapping:

$$\widetilde{\mathbf{x}}_h^{n+1,k} = \mathbf{x}_h^{bdf,n} + \frac{\Delta t}{\alpha_0}\left(\mathbf{v}_{h,W}^{n+1} + \widetilde{\Pi}_\Omega^{n+1,k}\, \mathbf{v}_{h,A}^{n+1} + \delta\widetilde{p}^{n+1,k}\, \mathbf{v}_{h,V}^{n+1}\right). \tag{3.23}$$

3. Check if the "guess" surface $\widetilde{\Omega}_{n+1}^k$ is sufficiently accurate, either by the stopping criteria based on the absolute area and volume conservation, as:

$$|J_A(\widetilde{\Omega}_{n+1}^k) - J_A(\Omega_n)| \le \tau_A^A \qquad \text{and} \qquad |J_V(\widetilde{\Omega}_{n+1}^k) - J_V(\Omega_n)| \le \tau_V^A, \tag{3.24}$$

respectively, or the criteria based on the relative area and volume, as:

$$\frac{|J_A(\widetilde{\Omega}_{n+1}^k) - J_A(\Omega_n)|}{J_A(\Omega_n)} \le \tau_A^R \qquad \text{and} \qquad \frac{|J_V(\widetilde{\Omega}_{n+1}^k) - J_V(\Omega_n)|}{J_V(\Omega_n)} \le \tau_V^R, \tag{3.25}$$

respectively, where τ_A^A, τ_V^A, τ_A^R, and $\tau_V^R \in \mathbb{R}$ are suitable tolerances. If the stopping criteria (3.24) or (3.25) are fulfilled, then stop the iterations, set $\Pi_\Omega^{n+1} = \widetilde{\Pi}_\Omega^{n+1,k}$ and $\delta p^{n+1} = \delta\widetilde{p}^{n+1,k}$, for which $\Omega_{n+1} = \widetilde{\Omega}_{n+1}^k$, and proceed to the following time step. Otherwise, continue to point 4.

4. Evaluate the Jacobian of $\mathbf{f}_c^n$ at step k as follows:

$$\mathrm{D}\,\mathbf{f}_c(\widetilde{\Pi}_\Omega^{n+1,k}, \delta\widetilde{p}^{n+1,k}) = \tag{3.26}$$
$$\frac{\Delta t}{\alpha_0}\begin{bmatrix} \displaystyle\int_{\widetilde{\Omega}_{n+1}^k} \nabla_{\widetilde{\Omega}_{n+1}^k} \cdot \mathbf{v}_{h,A}^{n+1}\, d\widetilde{\Omega}_{n+1}^k & \displaystyle\int_{\widetilde{\Omega}_{n+1}^k} \nabla_{\widetilde{\Omega}_{n+1}^k} \cdot \mathbf{v}_{h,V}^{n+1}\, d\widetilde{\Omega}_{n+1}^k \\ \displaystyle\int_{\widetilde{\Omega}_{n+1}^k} \mathbf{n}_{\widetilde{\Omega}_{n+1}^k} \cdot \mathbf{v}_{h,A}^{n+1}\, d\widetilde{\Omega}_{n+1}^k & \displaystyle\int_{\widetilde{\Omega}_{n+1}^k} \mathbf{n}_{\widetilde{\Omega}_{n+1}^k} \cdot \mathbf{v}_{h,V}^{n+1}\, d\widetilde{\Omega}_{n+1}^k \end{bmatrix}.$$

5. Solve the linear system:

$$\mathrm{D}\,\mathbf{f}_c(\widetilde{\Pi}_\Omega^{n+1,k}, \delta\widetilde{p}^{n+1,k}) \begin{bmatrix} \Delta\widetilde{\Pi}_\Omega^{n+1,k+1} \\ \Delta\delta\widetilde{p}^{n+1,k+1} \end{bmatrix} = \mathbf{f}_c(\widetilde{\Pi}_\Omega^{n+1,k}, \delta\widetilde{p}^{n+1,k}) \tag{3.27}$$

and update the Lagrangian multipliers as:

$$\begin{bmatrix} \widetilde{\Pi}_\Omega^{n+1,k+1} \\ \delta\widetilde{p}^{n+1,k+1} \end{bmatrix} = \begin{bmatrix} \widetilde{\Pi}_\Omega^{n+1,k} \\ \delta\widetilde{p}^{n+1,k} \end{bmatrix} - \rho \begin{bmatrix} \Delta\widetilde{\Pi}_\Omega^{n+1,k+1} \\ \Delta\delta\widetilde{p}^{n+1,k+1} \end{bmatrix}, \tag{3.28}$$

where $\rho \in \mathbb{R}$ is a relaxation parameter, which in this work we consider to be $\rho = 1$. Then, set $k = k + 1$ and continue from point 2 until convergence.

With this iterative method, we obtain the Lagrange multipliers Π_Ω^{n+1} and δp^{n+1} fulfilling the area and volume constraints by the surface Ω_{n+1} up to chosen tolerances. From now on, we will refer to this approach as *scheme C-1*.

3.3.2. Constraints enforcement: scheme C-2. To avoid solving a nonlinear problem at each time step, we impose the fulfillment of the area and volume constraints on the approximated surface Ω_* obtained by extrapolation. This is motivated by the accurate geometric representation offered by NURBS-based IGA. In particular, for all $n = 0, \dots, N-1$, we force the identity map $\mathbf{x}_h^{n+1}$ of the surface Ω_{n+1} to fulfill the following relations:

$$\int_{\Omega_*} H_h^* \, \mathbf{x}_h^{n+1} \cdot \mathbf{n}_{\Omega_*} \, d\Omega_* = A_0 \qquad \text{and} \qquad \int_{\Omega_*} \mathbf{x}_h^{n+1} \cdot \mathbf{n}_{\Omega_*} \, d\Omega_* = V_0. \tag{3.29}$$

By considering the area constraint and by using Eq. (3.14) we write:

$$\int_{\Omega_*} H_h^* \left(\mathbf{x}_h^{bdf,n} + \frac{\Delta t}{\alpha_0} \mathbf{v}_h^{n+1} \right) \cdot \mathbf{n}_{\Omega_*} \, d\Omega_* = A_0, \tag{3.30}$$

which becomes:

$$\int_{\Omega_*} H_h^* \, \mathbf{v}_h^{n+1} \cdot \mathbf{n}_{\Omega_*} \, d\Omega_* = \frac{\alpha_0}{\Delta t} \left(A_0 - \int_{\Omega_*} H_h^* \, \mathbf{x}_h^{bdf,n} \cdot \mathbf{n}_{\Omega_*} \, d\Omega_* \right). \tag{3.31}$$

Similarly, we rewrite the volume constraint as:

$$\int_{\Omega_*} \mathbf{v}_h^{n+1} \cdot \mathbf{n}_{\Omega_*} \, d\Omega_* = \frac{\alpha_0}{\Delta t} \left(V_0 - \int_{\Omega_*} \mathbf{x}_h^{bdf,n} \cdot \mathbf{n}_{\Omega_*} \, d\Omega_* \right). \tag{3.32}$$

Hereafter, with *scheme C-2* we will refer to problem (3.13) however with the equations related to the area and volume constraints replaced, for each $n = 0, \dots, N-1$, by Eqs. (3.31) and (3.32), respectively.

4. Numerical Results. In this section, we discuss the numerical results obtained by the approximation of the Canham–Helfrich problem on ellipsoids of different aspect ratio with the numerical scheme of Eq. (3.13), together with the two approaches, scheme C-1 and scheme C-2, introduced above.

We consider an initial geometry Ω_0 represented by an ellipsoid defined by:

$$\frac{x^2}{a_0^2} + \frac{y^2}{b_0^2} + \frac{z^2}{c_0^2} = 1 \qquad \{x, y, z\} \in \mathbb{R}^3, \tag{4.1}$$

with a_0, b_0 and $c_0 \in \mathbb{R}$ positive constants determining the aspect ratio of the ellipsoid. In the first case, we take $a_0 = 4$, $b_0 = 4$, and $c_0 = 1$ (which we refer to as *ellipsoid 4-4-1*), in the second one, we take $a_0 = 5$, $b_0 = 5$, and $c_0 = 1$ (which we call *ellipsoid 5-5-1*). For each of the two ellipsoids, we consider 4 different meshes: the first two

$t = 0$ $t = 0.08$ $t = 0.15$ $t = 0.45$ $t = 1.51$

Figure 2: Numerical approximation of the Canham–Helfrich flow of an ellipsoid Ω_0 with aspect ratio 4-4-1. Approximated surface Ω_n at different time instances, computed with the ref. 1 mesh built of NURBS basis functions of degree $p = 2$ and using scheme C-1.

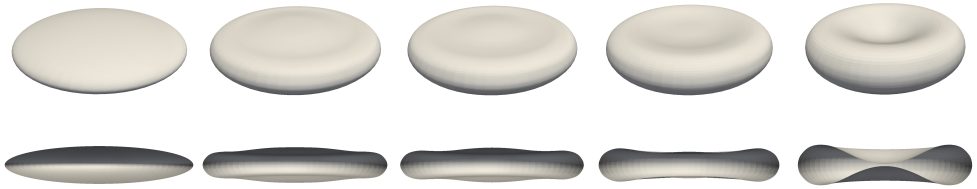

$t = 0$ $t = 0.06$ $t = 0.13$ $t = 0.38$ $t = 1.76$

Figure 3: Numerical approximation of the Canham–Helfrich flow of an ellipsoid Ω_0 with aspect ratio 5-5-1. Approximated surface Ω_n at different time instances, computed with the ref. 1 mesh built of NURBS basis functions of degree $p = 2$ and using scheme C-1.

built out of NURBS basis functions of polynomial degree $p = 2$, C^1-continuous a.e., for two refinement levels — yielding 684 elements and 2,048 total DOFs (*ref. 1*) and 2,380 elements and 8,192 total DOFs (*ref. 2*), respectively — and other two meshes built out of NURBS basis functions of degree $p = 3$, C^2-continuous a.e., for two refinement levels yielding 779 elements and 2,048 total DOFs (*ref. 1*) and 2,555 elements and 8,192 total DOFs (*ref. 2*), respectively. Regarding the time discretization, we present numerical results obtained using a BDF scheme of order $k = 2$ since it has already been shown to represent a good compromise between accuracy and computational cost for geometric PDEs in [27]. We consider a fixed time step size $\Delta t = 0.01$, and we set the constant $k_c = 1$.

In Figures 2 and 3 we report the approximated surfaces Ω_n at different time instances computed with the ref. 1 meshes built out of $p = 2$ degree NURBS basis functions and the scheme C-1 for the enforcement of the constraints, for the ellipsoid 4-4-1 and the ellipsoid 5-5-1, respectively. In both the cases, the biomembrane starts with an initial ellipsoid shape and converges to the typical biconcave shape of the red blood cells. The aspect ratio of the initial ellipsoid geometry sets the volume V_0 and area A_0 constraints. Then, also the final shape depends on the initial aspect ratio: considering Eq. (4.1), the higher a_0 and b_0 are with respect to c_0, the closer the two opposite sides of the biconcave shape tend to get.

In Figure 4, we report the evolution of the Willmore energy J_W with respect to time for all the meshes considered (ref. 1 and 2 for discretizations with NURBS of both degrees $p = 2$ and $p = 3$) and both the schemes C-1 and C-2. Similarly, we

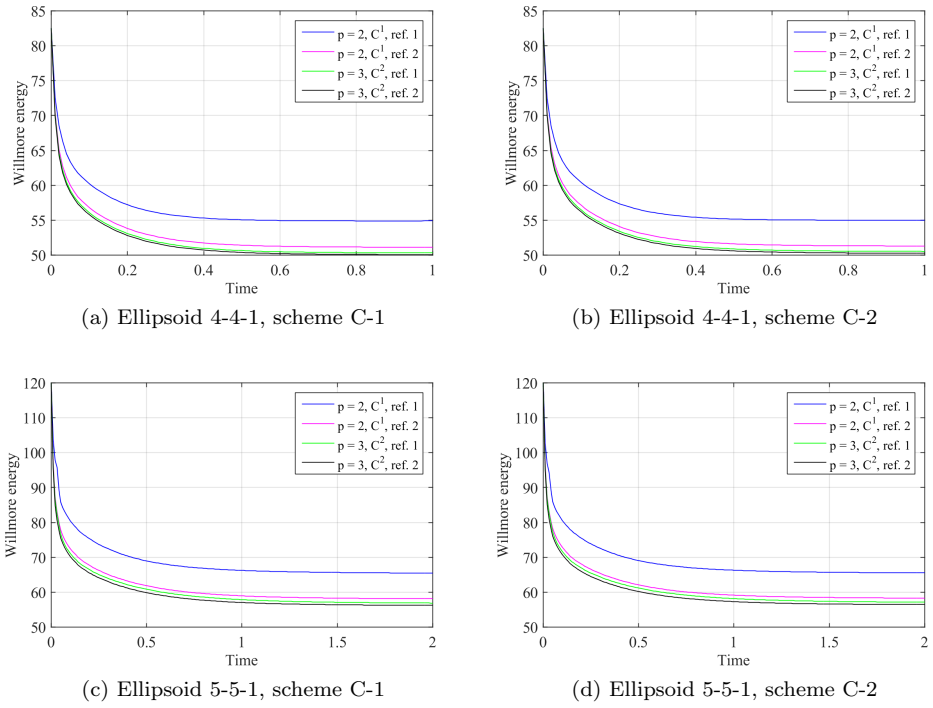

(a) Ellipsoid 4-4-1, scheme C-1

(b) Ellipsoid 4-4-1, scheme C-2

(c) Ellipsoid 5-5-1, scheme C-1

(d) Ellipsoid 5-5-1, scheme C-2

Figure 4: Numerical approximation of the Canham–Helfrich flow on ellipsoids of aspect ratio 4-4-1 (a) and (b), and 5-5-1 (c) and (d). Evolution of the Willmore energy J_W with respect to time, using meshes of two refinement levels built of NURBS of degrees $p = 2$ and $p = 3$, C^1- and C^2-continuous a.e., respectively, for schemes C-1 (a) and (c), and C-2 (b) and (d).

report in Figure 5 the evolution of the Lagrange multipliers Π_Ω^n and δp^n with respect to time for the same cases. In all the situations considered, the energy is minimized until it reaches a stable biconcave configuration with a more pronounced pinching in the center of the surface when a lower value of the Willmore energy J_W is reached. The results show a common trend: the Willmore energy is minimized to a smaller and smaller value as the polynomial degree p increases, the mesh is finer and the scheme for the enforcement of the constraints is more accurate.

Scheme C-1 is able to enforce the area and volume constraints within any prescribed tolerance. In this work, we choose the tolerance such that $|J_A(\Omega_n) - A_0| \leq 10^{-7}$ and $|J_V(\Omega_n) - V_0| \leq 10^{-7}$. The convergence of the quasi-Newton iterations to the final values of the Lagrange multipliers is fast, with a number of iterations usually between 1 and 3. Instead, the scheme C-2 described in Section 3.3.2 enforces the constraints only approximately. We report the evolution of the errors in area and volume of the approximated surfaces in Figure 6, for all the meshes considered, calculated as $e_A(t) = \dfrac{J_A(\Omega_t) - A_0}{A_0}$ and $e_V(t) = \dfrac{J_V(\Omega_t) - V_0}{V_0}$, respectively. The errors remain always positive vs. time, inferring an increment in area and volume of the approximated surfaces with respect to the initial one, mostly concentrated in the initial time steps of the simulations, where the evolution of the surface is faster. Nevertheless, these increments remain in practice "small": with respect to the initial surface, the area of the

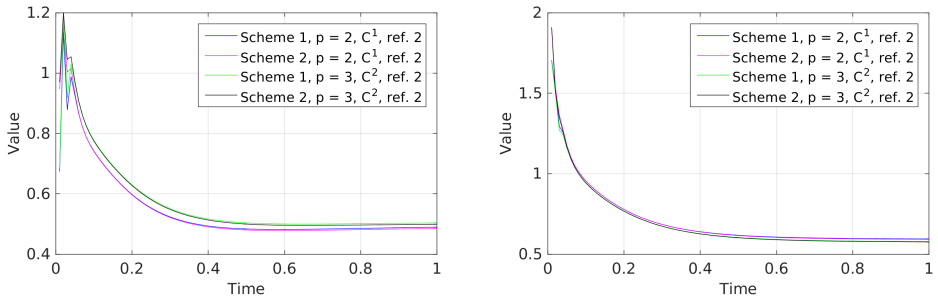

(a) Ellipsoid 4-4-1, area Lagrange multiplier Π_Ω (b) Ellipsoid 4-4-1, volume Lagrange multiplier δp

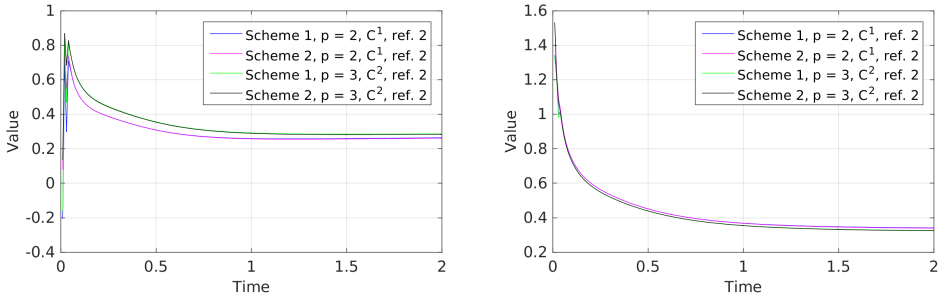

(c) Ellipsoid 5-5-1, area Lagrange multiplier Π_Ω (d) Ellipsoid 5-5-1, volume Lagrange multiplier δp

Figure 5: Numerical approximation of the Canham–Helfrich flow on ellipsoids of aspect ratio 4-4-1 (a) and (b), and 5-5-1 (c) and (d). Evolution of the Lagrange multipliers Π_Ω (a) and (c), and δp (b) and (d) for meshes of refinement level 2 built of NURBS of degrees $p = 2$ and $p = 3$, C^1- and C^2-continuous a.e., respectively, for schemes C-1 and C-2.

approximated surface is between $0.368 \div 0.408$ % larger, for the different NURBS cases of the ellipsoid 4-4-1, and between $0.441 \div 0.545$ % larger, for the ellipsoid 5-5-1; the volume is instead between $0.041 \div 0.049$ % larger, for the ellipsoid 4-4-1, and between $0.046 \div 0.051$ % larger, for the ellipsoid 5-5-1. We consider these errors acceptable, considering also the lower computational effort needed with scheme C-2 with respect to scheme C-1: indeed, the scheme C-1 involves the solution of 3 linear systems related to the problems of Eq. (3.19), which share the same left-hand-side but have different right-hand-sides, followed by the iterative procedure to find the roots of the function of Eq. (3.20), whose Jacobian is costly to compute. The scheme C-2, instead, leads to a linear system that stems from the discretized formulation of Eq. (3.13) with two additional unknowns, the Lagrange multipliers Π_Ω^n and δp^n, which leads to a bigger (and slightly harder) linear system to solve, but still faster to treat than the whole procedure required for scheme C-1. Basically, with scheme C-2 we gain performance in exchange of lower accuracy, while with scheme C-1 we obtain the best accuracy we can have (up to machine precision) at the cost of a more costly and involved procedure to follow.

5. Conclusions. In this paper, we studied the numerical approximation of the geometric PDE yielding the minimization of the Canham–Helfrich energy, a continuum model for the shape at equilibrium of lipid biomembranes, and in particular of

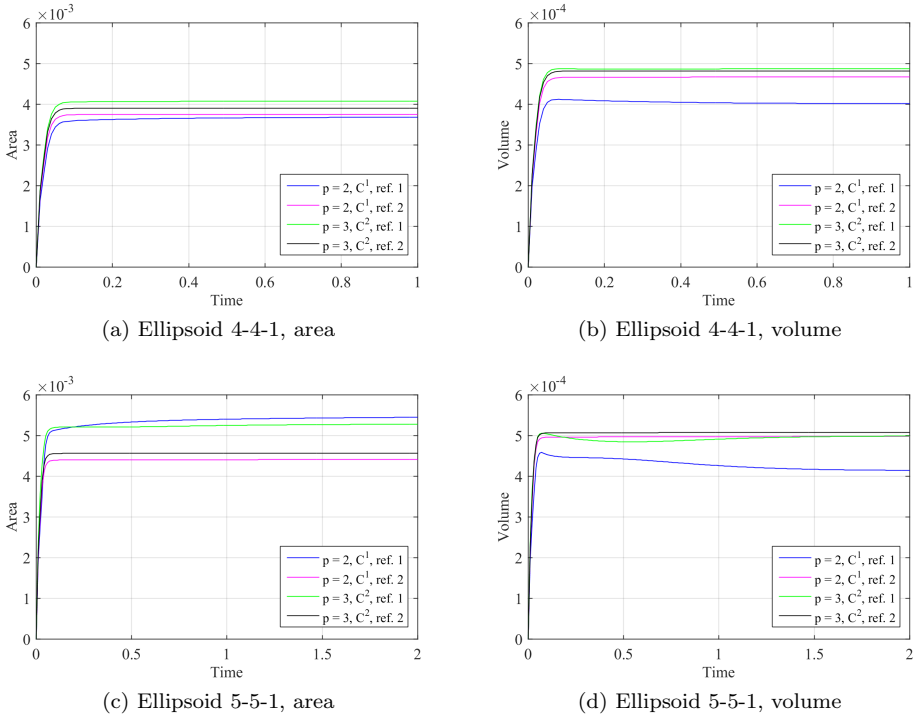

(a) Ellipsoid 4-4-1, area (b) Ellipsoid 4-4-1, volume

(c) Ellipsoid 5-5-1, area (d) Ellipsoid 5-5-1, volume

Figure 6: Numerical approximation of the Canham–Helfrich flow on ellipsoids of aspect ratio 4-4-1 (a) and (b), and 5-5-1 (c) and (d). Errors e_A (a) and (c), and e_V (b) and (d) in area and volume preservation with respect to time, for meshes of two refinement levels built of NURBS of degrees $p = 2$ and $p = 3$, C^1- and C^2-continuous a.e., respectively, employing the scheme C-2.

red blood cells. This leads to a highly nonlinear, high order surface PDE, involving geometric quantities such as the normal and the curvature of the surface, which are usually difficult to treat numerically with standard approaches based on the Finite Element Method. We discussed the spatial discretization of this PDE by means of NURBS-based IGA in the framework of the Galerkin method. In this regard, we proposed a formulation based on the velocity and the normal velocity of the points of the surface already introduced in our previous work [27] and coupled with two Lagrange multipliers for the treatment of the area and volume constraints. As in [27], we discretized the PDEs in time by employing high order BDF schemes, with explicit treatment of the extrapolated geometric quantities. We also considered two schemes for the enforcement of the constraints. The first one, in Section 3.3.1, is an adaptation of the iterative scheme described in [31] to the discretization based on IGA and BDF schemes, while for the second one, described in Section 3.3.2, the area and volume constraints are enforced on the extrapolated surface. We reported results of the numerical approximation of the Canham–Helfrich flow on geometries with initial ellipsoidal shape of aspect ratio 4-4-1 and 5-5-1, respectively. In both the cases, the minimization of the Canham–Helfrich energy results in the surface evolving towards the typical biconcave shape of red blood cells. We compared the results obtained with different discretizations, based on NURBS of polynomial degrees $p = 2$ and $p = 3$,

with basis functions C^1- and C^2-continuous a.e., respectively, for two refinements levels. We showed that, thanks to the spatial and time accuracy of the proposed formulation, even with a small amount of DOFs, we obtain a satisfactory approximated surface and minimization of the Canham–Helfrich energy for the considered geometries. Moreover, we compared the two schemes for the enforcement of the area and volume constraints. With the first scheme, the area and the volume are preserved within a selectable tolerance, thus potentially up to machine precision. With the second scheme, we have a relatively small conservation error, but at reduced computational cost. We remark that this second way of enforcing the constraints is feasible only thanks to the high accuracy of the spatial discretization and extrapolation of the surface, made possible by the adoption of NURBS-based IGA.

Acknowledgments. The authors acknowledge the financial support of the Swiss National Science Foundation through the project "Isogeometric Analysis for Partial Differential Equations: surface models and optimization problems in Haemodynamics" (project 147033), 2014–2016.

REFERENCES

[1] U. Seifert, Configurations of fluid membranes and vesicles, Advances in Physics 46 (1) (1997) 13–137.
[2] B. Alberts, D. Bray, J. Lewis, M. Raff, K. Roberts, J. D. Watson, Molecular biology of the cell, 3rd ed., Garland, New York, 1994.
[3] S. K. Boey, D. H. Boal, D. E. Discher, Simulations of the erythrocyte cytoskeleton at large deformation. I. Microscopic models, Biophysical Journal 75 (3) (1998) 1573–1583.
[4] D. E. Discher, D. H. Boal, S. K. Boey, Simulations of the erythrocyte cytoskeleton at large deformation. II. Micropipette aspiration, Biophysical Journal 75 (3) (1998) 1584–1597.
[5] J. Li, M. Dao, C. T. Lim, S. Suresh, Spectrin-level modeling of the cytoskeleton and optical tweezers stretching of the erythrocyte, Biophysical Journal 88 (5) (2005) 3707–3719.
[6] H. Noguchi, G. Gompper, Shape transitions of fluid vesicles and red blood cells in capillary flows, Proceedings of the National Academy of Sciences of the United States of America 102 (40) (2005) 14159–14164.
[7] D. A. Fedosov, B. Caswell, G. E. Karniadakis, A multiscale red blood cell model with accurate mechanics, rheology, and dynamics, Biophysical Journal 98 (10) (2010) 2215–2225.
[8] D. A. Fedosov, H. Lei, B. Caswell, S. Suresh, G. E. Karniadakis, Multiscale modeling of red blood cell mechanics and blood flow in malaria, PLOS Computational Biology 7 (12) (2011) 1–13.
[9] D. Hartmann, A multiscale model for red blood cell mechanics, Biomechanics and Modeling in Mechanobiology 9 (1) (2010) 1–17.
[10] M. S. Pauletti, Parametric AFEM for geometric evolution equation and coupled fluid-membrane interaction, Ph.D. thesis, University of Maryland (2008).
[11] P. Morin, R. H. Nochetto, M. S. Pauletti, M. Verani, AFEM for shape optimization, MOX Report, Politecnico di Milano 29 (2011).
[12] A. Bonito, R. H. Nochetto, M. S. Pauletti, Parametric FEM for geometric biomembranes, Journal of Computational Physics 229 (9) (2010) 3171–3188.
[13] A. Bonito, R. H. Nochetto, M. S. Pauletti, Dynamics of biomembranes: effect of the bulk fluid, Mathematical Modelling of Natural Phenomena 6 (05) (2011) 25–43.
[14] A. Laadhari, C. Misbah, P. Saramito, On the equilibrium equation for a generalized biological membrane energy by using a shape optimization approach, Physica D: Nonlinear Phenomena 239 (16) (2010) 1567–1572.
[15] H. Casquero, C. Bona-Casas, H. Gomez, NURBS-based numerical proxies for red blood cells and circulating tumor cells in microscale blood flow, Computer Methods in Applied Mechanics and Engineering (2016), doi:http://dx.doi.org/10.1016/j.cma.2016.09.031.
[16] Y. Fung, Biomechanics: Mechanical properties of living tissues, Springer-Verlag, Berlin and Heidelberg, 1993.
[17] W. Helfrich, Elastic properties of lipid bilayers: theory and possible experiments, Zeitschrift für Naturforschung. Teil C 28 (11) (1973) 693–703.
[18] P. B. Canham, The minimum energy of bending as a possible explanation of the biconcave

shape of the human red blood cell, Journal of Theoretical Biology 26 (1) (1970) 61–81.
[19] Q. Du, C. Liu, X. Wang, A phase field approach in the numerical study of the elastic bending energy for vesicle membranes, Journal of Computational Physics 198 (2) (2004) 450–468.
[20] Q. Du, L. Zhu, Analysis of a mixed finite element method for a phase field bending elasticity model of vesicle membrane deformation, Journal of Computational Mathematics 24 (3) (2006) 265–280.
[21] X. Wang, Q. Du, Modelling and simulations of multi-component lipid membranes and open membranes via diffuse interface approaches, Journal of Mathematical Biology 56 (3) (2008) 347–371.
[22] J. A. Cottrell, T. J. R. Hughes, Y. Bazilevs, Isogeometric Analysis: Toward Integration of CAD and FEA, John Wiley & Sons, 2009.
[23] T. J. R. Hughes, J. A. Cottrell, Y. Bazilevs, Isogeometric Analysis: CAD, finite elements, NURBS, exact geometry and mesh refinement, Computer Methods in Applied Mechanics and Engineering 194 (39) (2005) 4135–4195.
[24] L. A. Piegl, W. Tiller, The NURBS Book, Springer-Verlag, Berlin, 1997.
[25] A. Tagliabue, L. Dedè, A. Quarteroni, Isogeometric Analysis and error estimates for high order partial differential equations in fluid dynamics, Computers & Fluids 102 (2014) 277–303.
[26] A. Bartezzaghi, L. Dedè, A. Quarteroni, Isogeometric Analysis of high order partial differential equations on surfaces, Computer Methods in Applied Mechanics and Engineering 295 (2015) 446–469.
[27] A. Bartezzaghi, L. Dedè, A. Quarteroni, Isogeometric Analysis of geometric Partial Differential Equations, Computer Methods in Applied Mechanics and Engineering 311 (2016) 625–647.
[28] A. Quarteroni, R. Sacco, F. Saleri, Numerical Mathematics, Springer-Verlag, Berlin and Heidelberg, 2007.
[29] P. Gervasio, F. Saleri, A. Veneziani, Algebraic fractional-step schemes with spectral methods for the incompressible Navier–Stokes equations, Journal of Computational Physics 214 (1) (2006) 347–365.
[30] D. Forti, L. Dedè, Semi-implicit BDF time discretization of the Navier–Stokes equations with VMS–LES modeling in a High Performance Computing framework, Computers & Fluids 117 (2015) 168–182.
[31] A. Bonito, R. H. Nochetto, M. S. Pauletti, Geometrically consistent mesh modification, SIAM Journal on Numerical Analysis 48 (5) (2010) 1877–1899.
[32] T. J. Willmore, Riemannian Geometry, Oxford University Press, 1996.
[33] W. Helfrich, Blocked lipid exchange in bilayers and its possible influence on the shape of vesicles, Zeitschrift für Naturforschung. Teil C 29 (9-10) (1974) 510–515.
[34] H. J. Deuling, W. Helfrich, Red blood cell shapes as explained on the basis of curvature elasticity, Biophysical Journal 16 (8) (1976) 861.
[35] B. Seguin, E. Fried, Microphysical derivation of the Canham–Helfrich free-energy density, Journal of Mathematical Biology 68 (3) (2014) 647–665.
[36] M. P. Do Carmo, Differential geometry of curves and surfaces, Vol. 2, Prentice-Hall, Englewood Cliffs (NJ), 1976.
[37] O.-Y. Zhong-Can, W. Helfrich, Bending energy of vesicle membranes: General expressions for the first, second, and third variation of the shape energy and applications to spheres and cylinders, Physical Review A 39 (10) (1989) 5280.
[38] G. Dziuk, Computational parametric Willmore flow, Numerische Mathematik 111 (1) (2008) 55–80.
[39] R. E. Rusu, An algorithm for the elastic flow of surfaces, Interfaces and Free Boundaries 7 (3) (2005) 229–239.
[40] L. Dedè, A. Quarteroni, Isogeometric Analysis for second order Partial Differential Equations on surfaces, Computer Methods in Applied Mechanics and Engineering 284 (2015) 807–834.
[41] J. W. Barrett, H. Garcke, R. Nürnberg, Parametric approximation of Willmore flow and related geometric evolution equations, SIAM Journal on Scientific Computing 31 (1) (2008) 225–253.
[42] G. S. Rao, Numerical Analysis, New Age International Publishers, New Delhi, 2009.

MOX Technical Reports, last issues

Dipartimento di Matematica
Politecnico di Milano, Via Bonardi 9 - 20133 Milano (Italy)

21/2017 Talska, R.; Menafoglio, A.; Machalova, J.; Hron, K.; Fiserova, E.
Compositional regression with functional response

18/2017 Ambartsumyan, I.; Khattatov, E.; Yotov, I.; Zunino, P.
A Lagrange multiplier method for a Stokes-Biot fluid-poroelastic structure interaction model

19/2017 Giovanardi, B.; Formaggia, L.; Scotti, A.; Zunino P.
Unfitted FEM for modelling the interaction of multiple fractures in a poroelastic medium

20/2017 Albrecht G.; Caliò F.; Miglio E.
Fair surface reconstruction through rational triangular cubic Bézier patches

16/2017 Ghiglietti, A.; Scarale, M.G.; Miceli, R.; Ieva, F.; Mariani, L.; Gavazzi, C.; Paganoni, A.M.; E
Urn models for response-adaptive randomized designs: a simulation study based on a non-adaptive randomized trial

15/2017 Tagliabue, A; Dede', L.; Quarteroni A.
Complex blood flow patterns in an idealized left ventricle: a numerical study

14/2017 Bruggi, M.; Parolini, N.; Regazzoni, F.; Verani, M.
Finite Element approximation of an evolutionary Topology Optimization problem

13/2017 Gigante, G.; Vergara, C.
Optimized Schwarz Methods for circular flat interfaces and geometric heterogeneous coupled problems

17/2017 Agosti, A.
Error Analysis of a finite element approximation of a degenerate Cahn-Hilliard equation

12/2017 Gasperoni, F.; Ieva, F.; Barbati, G.; Scagnetto, A.; Iorio, A.; Sinagra, G.; Di Lenarda, A.
Multi state modelling of heart failure care path: a population-based investigation from Italy